# Modeling of Biomolecular Systems with the Quantum Mechanical and Molecular Mechanical Method Based on the Effective Fragment Potential Technique: Proposal of Flexible Fragments

**Bella L. Grigorenko,**[†] **Alexander V. Nemukhin,**[†] **Igor A. Topol,**[*,‡] **and Stanley K. Burt**[‡]

*Chemistry Department, M. V. Lomonosov Moscow State University, Moscow 119899, Russian Federation, and Advanced Biomedical Computing Center, SAIC Frederick, National Cancer Institute at Frederick, P. O. Box B, Frederick, Maryland 21702*

Development and applications of a new approach to hybrid quantum mechanical and molecular mechanical (QM/MM) theory based on the effective fragment potential (EFP) technique for modeling properties and reactivity of large molecular systems of biochemical significance are described. It is shown that a restriction of frozen internal coordinates of effective fragments in the original formulation of the theory (Gordon, M. S.; Freitag, M. A.; Bandyopadhyay, P.; Jensen, J. H.; Kairys, V.; Stevens, W. J. *J. Phys. Chem. A* **2001,** *105,* 293) can be removed by introducing a set of small EFs and replacing the EFP−EFP interactions by the customary MM force fields. The concept of effective fragments is also utilized to solve the QM/MM boundary problem across covalent bonds. The buffer fragment, which is common for both subsystems, is introduced and treated specially when energy and energy gradients are computed. An analysis of conformations of dipeptide−water complexes, as well as of dipepties with His and Lys residues, confirms the reliability of the theory. By using the Hartree−Fock and MP2 quantum chemistry methods with the OPLS-AA molecular mechanical force fields, we calculated the energy difference between the enzyme−substrate complex and the first tetrahedral intermediate for the model active site of the serine protease catalytic system. In another example, the multiconfigurational complete active space self-consistent field (CASSCF) method was used to model the homolytic dissociation of the peptide helix over the central C−N bonds. Finally, the potentials of internal rotation of the water dimer considered as a part of the water wire inside a polyglycine analogue of the ion channel gramicidin A were computed. In all cases, an importance of the peptide environment from MM subsystems on the computed properties of the quantum parts is demonstrated.

## 1. Introduction

The use of hybrid quantum mechanical and molecular mechanical (QM/MM) methods to characterize properties of large molecular systems and to model chemical reactions in condensed media has gained increasing attention in recent years. A number of successful realizations of the idea to describe a central part of the entire molecular system at the QM level and the environmental part by the MM options are extensively presented in the literature.[1−27] However, more efforts are still needed to create a tool that will allow one to apply this technique routinely like conventional quantum chemistry methods. A major obstacle toward this goal is a treatment of the boundary region between the QM and MM subsystems.

Among various approaches to QM/MM methods, the scheme based on the effective fragment potential (EFP) technique[13−27] offers certain advantages. In this approach, the QM−MM interaction is modeled by interactions of QM atoms with the effective fragments, representing groups of atoms from the MM part. The corresponding interactions can be computed with the help of the well-known quantum chemistry program system GAMESS.[28] The majority of parameters describing EFPs can be principally found from separate ab initio calculations instead of using empirical adjustments. Several successful applications

of the EFP-based QM/MM method have been described in the literature, among which we distinguish the approaches to study biomolecules.[17−27]

Krauss et al.[17−23] modeled the stages of some enzyme-catalyzed reactions by partitioning the systems into active quantum regions, which consisted of a fairly restricted number of atoms, and EFP spectator regions. The position of all atoms in the effective fragments was kept fixed in positions obtained from crystallographical studies. In attempts to handle the QM/MM boundary across covalent bonds, Kairys and Jensen suggested the introduction of a buffer region to separate QM and MM(EFP) subsystems, which was described with help of frozen localized molecular orbitals.[24] This idea was successfully developed in a series of simulations carried out in the Jensen group.[25−27] It was also suggested[25] to partition a single large effective fragment, representing the MM part, into several overlapping but still extended pieces to provide a practical tool to generate ab initio EFP parameters.

In all EFP approaches, the effective fragments are assumed to be geometrically frozen during chemical transformations in the quantum area. Such a restriction is an obvious shortcoming when modeling biomolecular systems, because conformational changes in the MM part, which accompany chemical reactions in the QM site, may seriously affect energy profiles.

Recently, we described an approach to the EFP-based QM/MM theory that is free from such limitation and applied it to systems in which the QM/MM boundary extended across the

* To whom correspondence should be addressed.
† M. V. Lomonosov Moscow State University.
‡ National Cancer Institute at Frederick.

hydrogen bonds.[29] In the present paper, we show the results that demonstrate capabilities of this technique for modeling systems subdivided into the QM and MM parts across covalent bonds as well. In our method, we consider the MM subsystem as connected chains of small effective fragments, calculate their interactions with the QM part as in customary EFP methods, but replace fragment−fragment interactions by interactions dictated by MM force fields. By doing such a replacement, we provide enough flexibility to the MM subsystem toward conformational changes.

We also explore the idea of a buffer region separating QM and MM parts across covalent bonds and use localized molecular orbitals for its description but suggest an original treatment of the buffer. Namely, in our model, the buffer is a special effective fragment common to both subsystems. Such an approach turns out to be very helpful in attempts to solve the boundary problem. A combination of the molecular modeling programs GAMESS[28] (or properly modified PC GAMESS[30]) and TINKER[31] provides a technical realization for this QM/MM scheme.

A detailed description of the method is presented in section 2. We also include in this section a new study of dipeptide−water complexes, as well as an analysis of conformations and proton affinities of dipepties with His and Lys residues. These results demonstrate the reliability of the theory.

In section 3, we show applications of the new technique to three different problems, in which various quantum chemistry methods are applied to the QM part while peptide environments are described by OPLS-AA molecular mechanical force fields. In the first example, we calculated the minimum energy structures and estimated the energy difference between the enzyme−substrate complex and the first tetrahedral intermediate for the model active site of the serine protease catalytic system by using the Hartree−Fock and MP2 methods. In another example, the multiconfigurational complete active space self-consistent field (CASSCF) method was used to model the homolytic dissociation of the peptide helix over one of the central C−N bonds. In the last example, the Hartree−Fock potentials of internal rotation of the water dimer, considered as a part of the water wire inside a polyglycine analogue of the ion channel gramicidin A, were computed. In all cases, we focused on the role of the peptide environment on the computed properties of the QM subsystem.

## 2. The Method

In the EFP method, the Hamiltonian of the molecular system composed of the ab initio part (solute species) and the environmental part (effective fragments standing for solvent species) may be written as[14]

$$\mathbf{H} = \mathbf{H}_{AR} + \mathbf{V} \qquad (1)$$

Here, $\mathbf{H}_{AR}$ refers to the ab initio region of the system and $\mathbf{V}$ represents the potential due to the effective fragments. In the original EFP formulation, the latter is expressed as a sum of electrostatic, polarization, and exchange-repulsion potentials depending on the electronic coordinates. Similar terms are added to describe the interactions between the nuclei in the ab initio and fragment molecules, as well as the fragment−fragment interactions. The energy of the entire molecular system is computed as a sum of ab initio energy originating from $\mathbf{H}_{AR}$ and interaction energy originating from $\mathbf{V}$.

As stated in the Introduction, we propose to consider the MM subsystem as a connected collection of relatively small effective
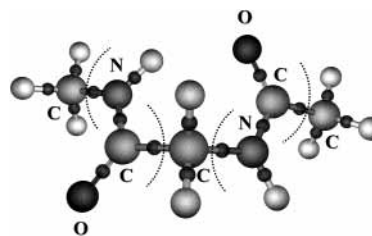


**Figure 1.** Partitioning of a typical segment of the MM subsystem into effective fragments.

fragments and to replace fragment−fragment interactions, routinely computed in GAMESS, by the force fields described by MM options. Therefore, the energy is computed as a sum of ab initio energy, interaction energies of ab initio particles with effective fragments, and interaction energies of groups of atoms from effective fragments modeled by MM force fields.

**Partitioning of the MM Subsystem.** In Figure 1, we show a typical segment of the MM part to be described by the effective fragment potential technique. Our proposal is to consider the MM subsystem not as a single effective fragment[17−23] or a fragment composed of overlapping large molecular pieces[25−27] but as a flexible chain of small EFs. An illustrative example of Figure 1 shows six effective fragments constituting the MM subsystem: two groups of $CH_3$, two of $C(O)N(H)$, and one of $CH_2$. Consistent with the EFP methodology, internal coordinates of these small fragments are assumed to be fixed, but their relative positions in the peptide chain are determined by MM force fields. For most applications, the assumption of frozen geometry of carefully selected small fragment units should not lead to serious errors.

According to the implementation of the EFP method in GAMESS, [28] the electrostatic potential acting on the quantum subsystem is represented by distributed multipoles centered at each atom and each bond midpoint. In Figure 1, the latter expansion points are marked by small black circles. The multipole expansions are extended from charges up to octupoles, and the corresponding parameters can be created in preliminary ab initio calculations using GAMESS. The exchange-repulsion interaction between an effective fragment and a quantum subsystem is modeled by one-electron potentials contributing to the ab initio Hamiltonian matrix. These potentials have the form of Gaussian functions located at atomic centers

$$\mathbf{V}^{REP}(\mathbf{r}) = \sum_{\mathbf{m}=1}^{\mathbf{M}} \sum_{\mathbf{k}=1}^{\mathbf{k}_{max}} \mathbf{c}_{\mathbf{mk}} \exp(-\alpha_{\mathbf{mk}}\mathbf{r}_{\mathbf{m}}^{2}) \qquad (2)$$

and the corresponding parameters $\mathbf{c}_{\mathbf{mk}}$ and $\alpha_{\mathbf{mk}}$ should be optimized by some fitting procedure.

In our first implementation of the flexible effective fragment potential QM/MM method,[29] we kept the polarization contributions to EFP and fitted parameters of the exchange-repulsive potentials within such construct. However, lately we found that essentially the same results for the intermolecular complexes described by the EFP-based QM/MM technique could be obtained by omitting the polarization terms and readjusting parameters of repulsive potentials for this scheme. In such approach, the empirically parametrized MM force fields take care of the solvent−solvent polarization effects and the polarization contributions to the solute−solvent interactions are implicitly taken into account through the properly fitted parameters of potentials $\mathbf{V}^{REP}$ (eq 2). Although in this scheme the latter actually lose the meaning of purely repulsive terms, we keep the same designation, $\mathbf{V}^{REP}$, as in the original EFP formulation.

Modeling of Biomolecular Systems

*J. Phys. Chem. A, Vol. 106, No. 44, 2002* **10665**

A pragmatic value of this approach is that we avoid severe convergence problems when solving the Hartree−Fock equations with the Hamiltonian (eq 1) containing the polarization potentials in **V** and avoid additional screening parameters[14] in the electrostatic potentials.

Therefore, the expression for the one-electron potential from the $\mu$th effective fragment is as follows

$$\mathbf{V}_\mu(\mathbf{r}) = \sum_{k=1}^{K} \mathbf{V}_{\mu,k}^{ELEC}(\mathbf{r}) + \mathbf{V}_\mu^{REP}(\mathbf{r}) \qquad (3)$$

In eqs 2 and 3, **r** denotes electronic coordinates originating from the corresponding expansion points, **K** is the number of such expansion points for a distributed multipolar analysis. Explicit expression for the electrostatic potential $\mathbf{V}^{ELEC}(\mathbf{r})$ may be found in refs 13 and 14. The terms of eq 3 are added to the one-electron operators in the Hamiltonian of the ab initio subsystem.

**Fit of Parameters for the Exchange Repulsion Potentials.** We selected parameters $\mathbf{c_{mk}}$ and $\alpha_{mk}$ of the repulsion potentials of eq 2 for the most typical fragments representing amino acid side chains by the following procedure. For the biomolecules, description of hydrogen bonding seems to be of primary importance and, therefore, a water molecule can serve as a probing vehicle in the adjustment procedure. We considered a variety of directions along which the water molecule could reach an effective fragment and carried out ab initio calculations to provide reference data. The fitting procedure is essentially the same as described, for example, in refs 15 and 20. In this work, we utilized the computer code REPGEN[32] to perform the least-squares optimization of parameters for the potentials $\mathbf{V}^{REP}(\mathbf{r})$ (eq 2). The Hartree−Fock approximation with the conventional 6-31G** basis sets was used for creation of multipole expansion parameters in $\mathbf{V}^{ELEC}(\mathbf{r})$, as well as for the fitting procedure. Reference ab initio interaction energies have been calculated for the variety of geometry configurations. For exactly the same coordinates, the sets of QM/EFP interaction energies were produced and the best suited coefficients $\mathbf{c_{mk}}$ and $\alpha_{mk}$ were selected. We verified that the fitted parameters of $\mathbf{V}^{REP}(\mathbf{r})$ could be used in QM/MM calculations with more extended basis sets, as well as with other quantum chemical procedures.

The reliability of such parametrization is discussed in detail in our previous publication[29] devoted to the QM/MM(EFP) modeling of hydrogen-bonded complexes of the dipeptide *N*-acetyl-L-alanine *N′*-methylamide with water molecules. Here, we present an additional example for a QM−MM cut across hydrogen bond, illustrating, in particular, that omission of the polarization terms in EFPs does not lead to worsening results compared to the traditional application of this methodology.[15,16,29,33]

The panels of Figure 2 show three minimum energy geometry configurations of the dipeptide−water complex obtained as a result of full ab initio optimization, as well as of QM/MM optimization by assuming a QM description for the water molecule and MM(EFP) description for the dipeptide by using the OPLS-AA molecular mechanical parameters. In both cases, quantum calculations have been performed by the Hartree−Fock method with conventional 6-31G and 6-31G** basis sets. In Table 1, we compare the optimized intermolecular distances and such sensitive energy values as the energies of water molecule in the field of dipeptide. In the latter case, we subtracted from the total energy of the dipeptide−water complex the energy of dipeptide in its particular conformation, $E(\text{water})_{QM/MM} = E_{QM/MM}(\text{complex}) - E_{MM}(\text{dipeptide})$ or $E(\text{water})_{\text{ab initio}} = E_{\text{ab initio}}$-



**Figure 2.** Minimum energy geometry configurations for the dipeptide−water complex.

**TABLE 1: The Computed Properties of the Peptide−Water Complexes Shown in Figure 2[a]**

| | method | $d_1$ | $d_2$ | $d_3$ | $\Delta E$ |
|---|---|---|---|---|---|
| config a | QM(HF/6-31G)/MM(OPLSAA) | 1.87 | 3.36 | | −1.57 |
| | ab initio (HF/6-31G) | 1.88 | 3.39 | | |
| | QM(HF/6-31G**)/MM(OPLSAA) | 1.86 | 3.59 | | 0.25 |
| | ab initio (HF/6-31G**) | 2.00 | 3.41 | | |
| config b | QM(HF/6-31G)/MM(OPLSAA) | 2.07 | | 1.90 | −2.82 |
| | ab initio (HF/6-31G) | 1.93 | | 2.10 | |
| | QM(HF/6-31G**)/MM(OPLSAA) | 2.05 | | 2.02 | −1.70 |
| | ab initio (HF/6-31G**) | 2.02 | | 2.18 | |
| config c | QM(HF/6-31G)/MM(OPLSAA) | 1.96 | | 1.90 | −2.38 |
| | ab initio (HF/6-31G) | 1.82 | | 1.94 | |
| | QM(HF/6-31G**)/MM(OPLSAA) | 1.94 | | 1.97 | −0.38 |
| | ab initio (HF/6-31G**) | 1.97 | | 2.12 | |

[a] Distances $d_1$ (from carbonyl oxygen to water hydrogen), $d_2$ (from carbon to water oxygen), and $d_3$ (from hydrogen to water oxygen) are given in Å; the differences $\Delta E$ between QM/MM and ab initio energies of the water molecule in the field of dipeptide (see text for explanation) are given in kcal/mol.

(complex) $- E_{\text{ab initio}}(\text{dipeptide})$, and compare in Table 1 the corresponding differences $\Delta E = E(\text{water})_{QM/MM} - E(\text{water})_{\text{ab initio}}$.

We see that the discrepancies between QM/MM and full ab initio equilibrium intermolecular distances computed in this application are of the same order as usually obtained in the QM/MM models.[8,11] The QM/MM errors in the energy differences are within 3 kcal/mol for both basis sets. As discussed in detail in ref 29, the energy differences between various isomers of
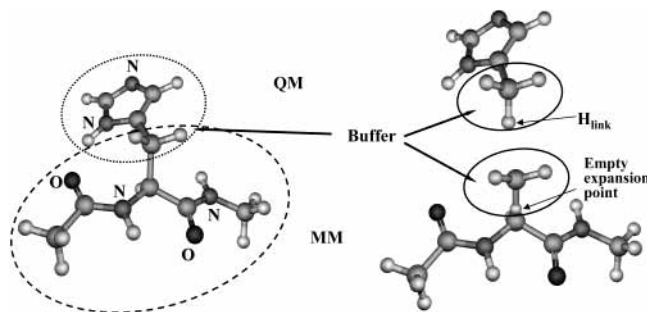
**Figure 3.** The scheme explaining treatment of the QM/MM boundary across a covalent bond and introduction of a buffer fragment.
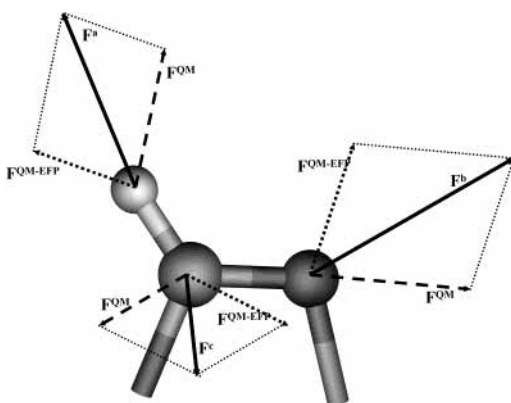


**Figure 4.** Calculation of forces in the QM part without buffer.

peptide−water complexes are computed in this QM/MM approach with the same accuracy.

**Treatment of the QM/MM Boundary across the $C_\alpha$−$C_\beta$ Bonds.** In Figure 3, we show an example of a molecular system to be partitioned into QM and MM parts across the covalent C−C bond. In this example, the dipeptide piece belongs to the MM subsystem and the histidine residue is to be described by quantum methods. The right panel of Figure 3 illustrates the same system as in the left panel but spatially separated for better understanding.

The key issue of the present method is an introduction of a buffer fragment as a group of atoms belonging to both QM and MM subsystems. Here, the $-CH_2-$ group is assigned to the buffer. We employ the usual maneuver to saturate the broken valence and add the link hydrogen atom to complete the QM subsystem, as shown in the upper right panel of Figure 3. Therefore, in the QM part, we distinguish the buffer (in this case, $CH_3$) as a special group of the quantum subsystem. The

same geometry configuration of the buffer fragment is assumed in the MM part. In the MM subsystem, which is a collection of effective fragments, the buffer is a special fragment as well. The position of the link atom is formally considered as an additional expansion point (as midbond points in "normal" effective fragments), which actually holds no multipoles. This trick, essentially based on the GAMESS implementation of the EFP method, helps us to keep the link atom precisely along the broken C−C bond during geometry optimizations of the entire system. In our scheme, this empty expansion point and the neighboring CH group of the MM peptide chain form an effective fragment, which interacts with the buffer fragment according to the MM force fields, and as a consequence, the link atom cannot leave the C−C axis.

When contributions to the one-electron Hamiltonian matrix of the QM subsystem from the MM(EFP) species are computed, the buffer fragment stays apart. These contributions are added only to the matrix elements of the quantum piece without buffer centers. We also attempt to describe the electronic density in the buffer region with the localized orbitals, keeping in mind that the approach of frozen localized orbitals in the region of immediate vicinity of the QM site is a helpful tool in treating the QM/MM boundary. We believe that the use of a minimal basis sets for buffer atoms is a reasonable first step in this direction.

The next three figures (Figures 4−6) illustrate the calculation scheme for the forces in all regions. As shown in Figure 4, for each atom (a, b, c, ...) in the QM part beyond buffer, the quantum forces $\mathbf{F}^{QM}$ (dashed lines) are combined with the forces acting on the QM atoms from effective fragments $\mathbf{F}^{QM−EFP}$ (dotted lines). Both types of forces are routinely computed in GAMESS.

In the left panel of Figure 5, we show the forces acting on the centers ($\alpha$, $\beta$, $\gamma$, ...) of an effective fragment in the MM subsystem (here the CONH fragment is presented as an example). Those are the forces arising from other MM fragments, $\mathbf{F}^{MM}$ (dashed lines), which act on the atoms. These quantities are computed by using the computer program TINKER. The forces from the QM subsystem, $\mathbf{F}^{EFP−QM}$ (dotted lines), act on the atomic centers and on the midbond expansion centers of this effective fragment as coded in GAMESS. As shown in the right panel of Figure 5, the forces acting on each center are summed up (bold lines) and finally applied to the center of mass of the fragment resulting in the total force, $\mathbf{F}$, and the total momentum, $\mathbf{M}$.

Figure 6 illustrates the treatment of the buffer region. As shown in the left panel, the forces from the quantum side, $\mathbf{F}^{QM}$
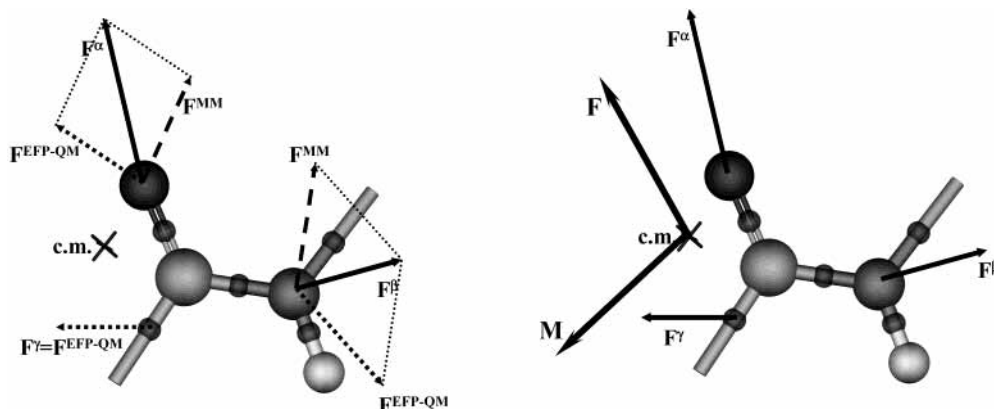


**Figure 5.** Calculation of forces in the effective fragments, representing the MM part, without buffer. A position of the center of mass (c.m.) is shown.

Modeling of Biomolecular Systems

*J. Phys. Chem. A, Vol. 106, No. 44, 2002* **10667**
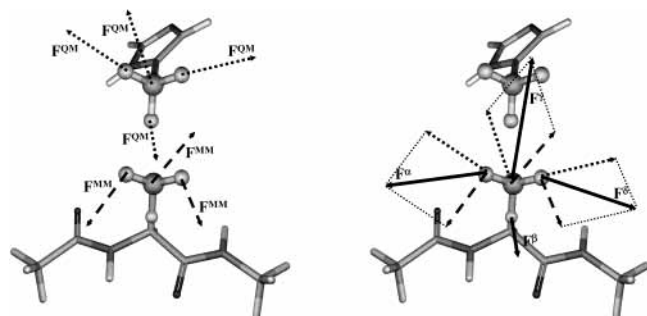


**Figure 6.** Calculation of forces acting on the buffer centers.

(dotted lines), are computed in GAMESS for all atoms including the link atom. The forces from other MM effective fragments, $\mathbf{F}^{MM}$ (dashed lines), are calculated in TINKER. The resulting forces (bold lines in the right panel) are declared as the forces contributing to two MM effective fragments. First is the $CH_2$ fragment, connecting pure QM and pure MM subsystems. Second is the fragment containing the empty expansion point at the position of link atom, where the quantum force is transferred, and the nearest CH group.

Finally, all energy contributions and energy gradients are collected in GAMESS, and the algorithms of this molecular modeling program are employed to find equilibrium geometry parameters of the entire QM/MM system.

To test this EFP-based QM/MM method with flexible fragments, we consider two examples, namely, the systems with histidine (His) and lysine (Lys) residues attached to the dipeptide chains. In both cases, we compare the results of complete geometry optimizations for two different isomers of each system at the ab initio (Hartree−Fock) and QM(Hartree−Fock)/MM-(OPLS-AA) levels with the basis sets 6-31G and 6-31G**, as well as the results for adiabatic proton affinities of the nitrogen centers. These examples provide very sensitive tests because protonation causes substantial changes in conformations of these species.

The structures of the His−dipeptide species shown in Figure 7 correspond to two notably different conformations (upper and lower panels), the energies of which differ by less than 2 kcal/mol. The QM/MM(OPLS-AA) calculations have been carried out by assuming the boundary cut across the $C_\alpha$−$C_\beta$ bond, as illustrated in Figure 3. The right panels (panels c and d) refer to the protonated species corresponding to those shown in panels a and b, respectively. We show the distances between oxygen in the MM part and hydrogen in the QM part, which are the most sensitive parameters to the computational procedure. One can see that the agreement between ab initio and QM/MM results is quite satisfactory.

The results for the natural charges obtained using the natural bond orbital (NBO) analysis[34] for the quantum subsystem at the QM/MM and ab initio levels (Table 2) prove that the distributions of electronic density in the quantum part are reproduced correctly in this hybrid approach.

Essentially the same conclusions may be drawn from the similar studies of the Lys−dipeptide structures, again with the QM/MM boundary across the $C_\alpha$−$C_\beta$ bond. We illustrate in Figure 8 the results obtained for one of the protonated isomers as a superposition of QM/MM and ab initio structures.

In Table 3, we collect the adiabatic proton affinities computed for two different conformations of the His−dipeptide and Lys−dipeptide species by using ab initio and QM/MM methods. In both cases, the quantum equations have been solved in the
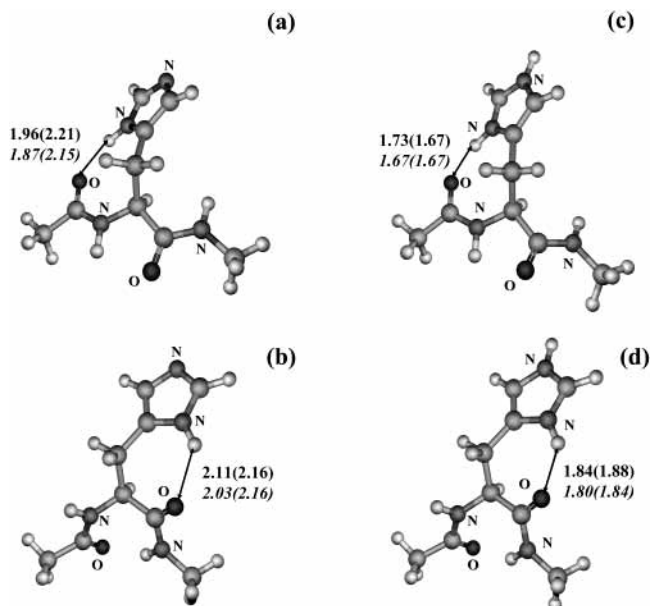


**Figure 7.** Equilibrium geometry configurations of the His−dipeptide systems. Panels a and b show two different conformers of the neutral species, while panels c and d show the corresponding protonated systems. Optimized distances in Å are given in the following order: upper rows present QM/MM(OPLS-AA) and ab initio (in parentheses) results at the HF/6-31G level; lower rows (in italics) refer to the same quantities but obtained at the HF/6-31G** level.

**TABLE 2: Natural Charges on Atoms of the Imidasole Ring of the His−Dipeptide System Computed at the Complete ab Initio (HF/6-31G**) and QM(HF/6-31G**)/MM(OPLS-AA) Levels**

| Species | Atom | Natural charges | |
|---|---|---|---|
| **Neutral form** | | QM/MM | *Ab initio* |
| | $C_{\delta2}$ | -0.151 | -0.125 |
| | $H_{\delta2}$ | 0.231 | 0.273 |
| | $N_{\epsilon2}$ | -0.543 | -0.535 |
| | $C_{\epsilon1}$ | 0.209 | 0.221 |
| | $H_{\epsilon1}$ | 0.231 | 0.232 |
| | $N_{\delta1}$ | -0.655 | -0.640 |
| | $H_{\delta1}$ | 0.510 | 0.486 |
| | $C_\gamma$ | -0.145 | 0.102 |
| **Protonated form** | | | |
| | $C_{\delta2}$ | -0.080 | -0.053 |
| | $H_{\delta2}$ | 0.280 | 0.282 |
| | $N_{\epsilon2}$ | -0.588 | -0.584 |
| | $H_{\epsilon2}$ | 0.490 | 0.489 |
| | $C_{\epsilon1}$ | 0.355 | 0.365 |
| | $H_{\epsilon1}$ | 0.284 | 0.283 |
| | $N_{\delta1}$ | -0.601 | -0.586 |
| | $H_{\delta1}$ | 0.574 | 0.534 |
| | $C_\gamma$ | -0.083 | 0.156 |

Hartree−Fock approximation with the basis sets 6-31G or 6-31G** and for the MM part the OPLS-AA parameters have been employed. With the exception of conformation 2 for Lys−dipeptide calculated with the smaller basis set, the errors of the QM/MM approach do not exceed 3 kcal/mol.

## 3. QM/MM Modeling

We present in this section the results of QM/MM modeling for three different systems by using different quantum chemistry

**10668** *J. Phys. Chem. A, Vol. 106, No. 44, 2002*

Grigorenko et al.
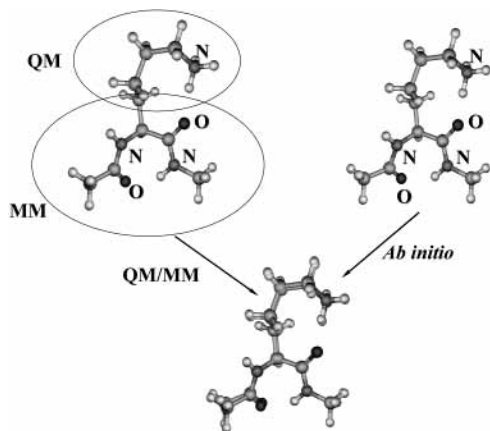


**Figure 8.** Comparison of the optimized QM/MM and ab initio conformations for the protonated form of the Lys−dipeptide system.

**TABLE 3: Adiabatic Proton Affinities (kcal/mol) of the His−Dipeptide and Lys−Dipeptide Species in Two Different Conformations as Computed at the ab Initio and QM/MM Levels**

| | Hartree−Fock/6-31G | | Hartree−Fock/6-31G** | |
|---|---|---|---|---|
| species | QM/MM | ab initio | QM/MM | ab initio |
| His, conform. 1 | 254 | 252 | 251 | 252 |
| His, conform. 2 | 253 | 253 | 250 | 253 |
| Lys, conform. 1 | 254 | 256 | 255 | 253 |
| Lys, conform. 2 | 250 | 259 | 252 | 254 |

approximations for the quantum part. Beyond demonstration of capabilities of the present QM/MM technique in these calculations, we focus on the effects caused by peptide environments on the parameters of the corresponding quantum parts. For this goal, we compare the computed properties for the entire QM/MM piece and for the quantum subsystem separated from the environment.

**Enzyme−Substrate and Intermediate State Complexes for the Serine Protease Catalytic Cycle.** An important field of applications of the QM/MM methods is modeling enzymatic reactions. The first example of the present QM/MM technique in this paper refers to the modeling of the reaction pathway in serine protease catalytic reactions.[35] Discussion of possible reaction mechanisms of this famous catalytic cycle is beyond the scope of the present paper,[36−39] and we only summarize here the features relevant to the present calculations.

The serine proteases are distinguished by a so-called catalytic triad in the active site, consisting of amino acids serine, histidine, and aspartic acid. The first step of the process is thought to proceed by a nucleophilic attack of the serine residue on the carbonyl carbon of substrate leading to formation of the so-called intermediate-state complex with a tetrahedral coordination of the carbon atom of the substrate. The path from the enzyme−substrate to the intermediate-state complex is supposed to be the rate-limiting stage of the entire catalytic cycle. As shown by quantum chemical calculations for simplified molecular models,[35,38,39] the configurations of the enzyme−substrate and the intermediate-state complexes correspond to the global and local minima on the potential energy surface of the model systems, and the energy gap between these two stationary points is fairly close to the transition state on the reaction path connecting these minima. In particular, in the Hartree−Fock calculations with the Stevens−Bash−Krauss effective core potentials and the corresponding basis sets, the barrier height was estimated[35] as 27.4 kcal/mol, while the tetrahedral inter-

mediate complex laid 21.0 kcal/mol above the global minimum. Single-point calculations along the same energy path at the B3LYP/6-31+G** density functional theory level resulted in the values 29.0 and 23.4 kcal/mol for the barrier and energy gap between minima, respectively.

Figure 9a illustrates the structure of the model enzyme−substrate complex optimized with the present QM/MM technique. The ball-and-stick representation is used to distinguish the QM part, and sticks are used to show the participants from the MM subsystem, which are flexible chains of effective fragments, as described in the previous section. The starting coordinates for the Ser-His-Asp triad, as well as for the additional moiety, asparagine, which plays an important role in stabilization of the intermediate-state complex (the so-called "oxyanion hole"), are borrowed from the experimental X-ray structure of proteinase K (entry 1IC6 of the Protein Data Bank).[40] As in our previous simulations,[35] the simplest substrate unit ($HCO-NH_2$) is chosen for these calculations. By performing full geometry optimization, we imposed the following restriction: all terminating $CH_3$ effective fragments in the MM chains were kept fixed in space, which allowed us to avoid artificial considerable replacements of separated (in this model) units Ser224, His69, Asp39, and Asn161 from their initial experimental positions. As seen in Figure 9, the flexible chains are fairly long, and such a restriction does not influence internal coordinates in the central part of the system. The optimized configuration of the central QM part is completely consistent with the findings of previous ab initio calculations.[35]

The structure of the intermediate-state complex, obtained as a point of a local minimum on the QM/MM potential energy surface, is shown in Figure 9b. Again, the arrangement of the atoms in the QM part is completely consistent with the previous knowledge;[35] namely, the proton from serine is transferred to histidine, the O(Ser)−C(substrate) distance is reduced from 2.46 to 1.56 Å, the initially planar configuration of substrate is distorted, and the C−O distance in substrate $CO-NH_2$ is increased from 1.23 to 1.31 Å.

Now we compare the energy differences $\Delta E$ between these two geometry configurations computed at various levels. The quantity $\Delta E$ computed in the QM(Hartree−Fock/6-31G)/MM-(OPLS-AA) approximation is 11.5 kcal/mol. If the Hartree−Fock/6-31G approach is applied only for the quantum subsystem subtracted from the MM environment (this means that all fragments shown in sticks are removed, and the link hydrogen atoms are kept in the buffer fragments), then we compute the energy difference as 24.3 kcal/mol. The latter quantity is fairly close to the results of the previous ab initio calculations[35] for approximately the same quantum system (21.0 kcal/mol). Therefore, we can attribute such a dramatic difference in the energy gap to the effect of the MM environment. We also recomputed the energies at the corresponding geometry configurations by using the MP2/6-31G** approximation for the QM part. For the QM/MM systems shown in Figure 9, we obtained for $\Delta E$ 17.1 kcal/mol, while for the subtracted quantum subsystem, this energy difference was 29.2 kcal/mol. Again, almost a 2-fold reduction of the energy gap is obtained due to effects of MM environment.

**Homolytic Dissociation of the Peptide Helix.** Calculations of reaction energy profiles often require the use of multiconfigurational quantum chemical approaches. For such example of our QM/MM modeling, we choose the dissociation of the helix, composed of 10 peptide groups, over one of the central

Modeling of Biomolecular Systems

*J. Phys. Chem. A, Vol. 106, No. 44, 2002* **10669**
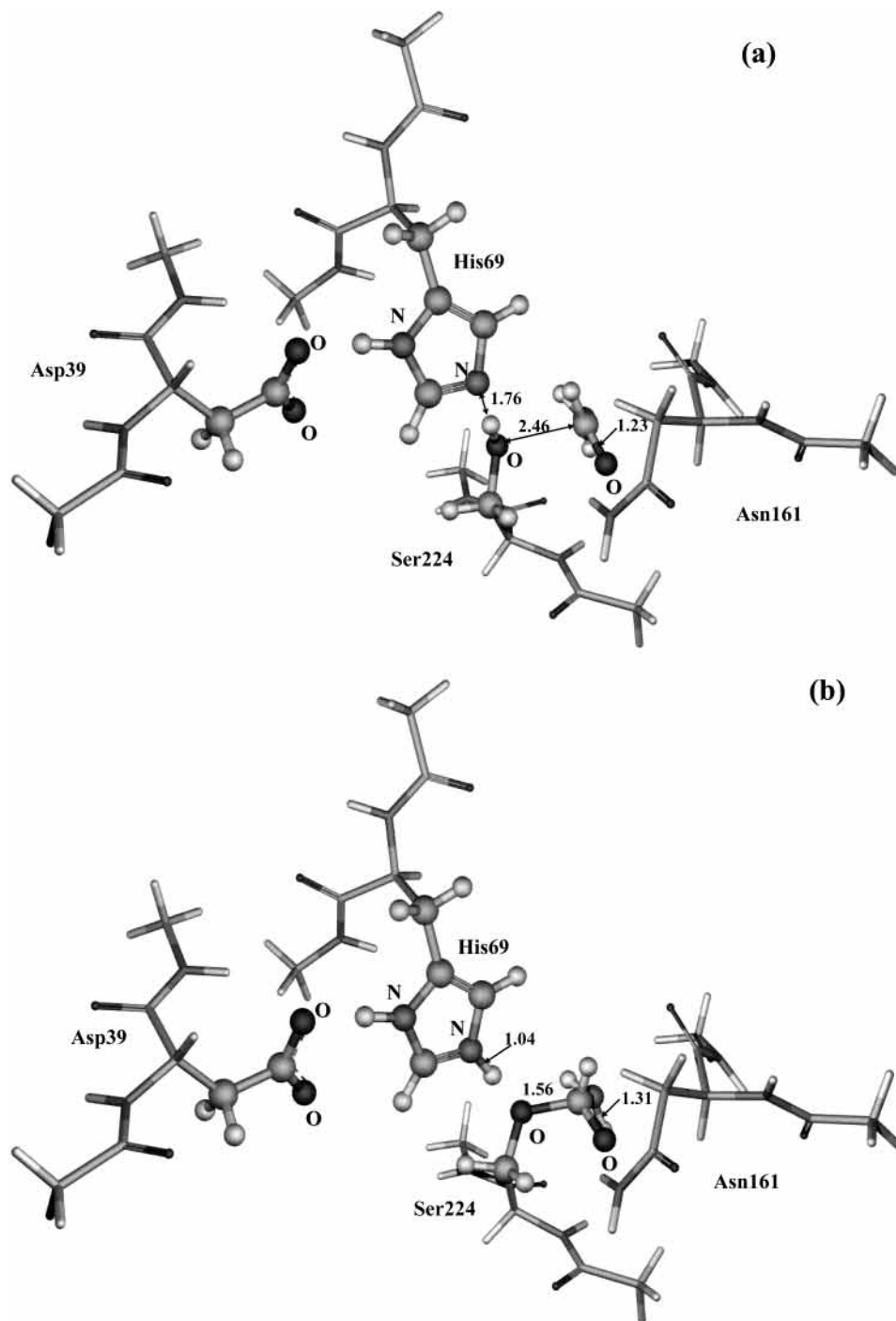


**Figure 9.** The structures of the model enzyme—substrate a and intermediate-state b complexes. Balls and sticks show the QM part; sticks refer to the MM part. Designation of residues corresponds to the experimental structure of proteinase K.[40] The equilibrium distances are given in Å.

C—N bonds. More specifically, we model the reaction that can be written as follows:

$$CH_3-(CO-NH-CH_2)_3-CO-NH-[CH_2-CO-NH-$$
$$CH_2]-CO-NH-(CO-NH-CH_2)_4-CH_3 \rightarrow CH_3-$$
$$(CO-NH-CH_2)_3-CO-NH-[CH_2-CO^\bullet] + [^\bullet NH-$$
$$CH_2]-CO-NH-(CO-NH-CH_2)_4-CH_3$$
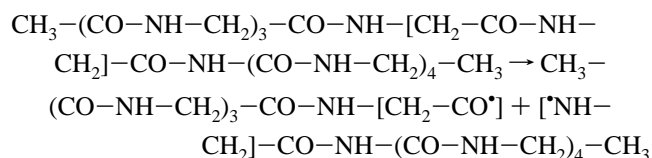
In this equation, the atoms in brackets constitute the QM part, the $CH_2$-groups being the buffer fragments, while all other groups form the MM part as flexible chains of effective fragments.

The initial equilibrium geometry configuration of the initial structure, obtained as a minimum energy point of the entire QM-(HF/6-31G)/MM(OPLS-AA) system, corresponded to a helix, parameters of which were fairly close, for example, to those of pure MM prediction with the molecular modeling program TINKER.

To model the dissociation reaction leading to two radicals $R-CO^\bullet + {}^\bullet NH-R'$ from the initial closed shell electronic structure, we performed the multiconfigurational complete active space self-consistent field (CASSCF) calculations with our QM/MM system. We used an approach based on the transformation from canonical molecular orbitals to natural bond orbitals (NBO) to be inserted into multiconfigurational expansions for the wave
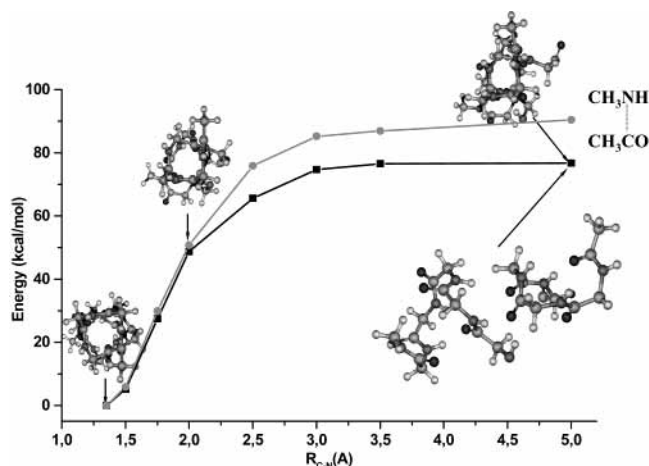
**Figure 10.** CASSCF energy profiles for the dissociation along the C–N bond in the QM/MM helix (the line with squares) and in the ab initio species $CH_3$–CO–NH–$CH_3$ (the line with circles).

functions. [41] In doing such, we can precisely distinguish the orbitals responsible for this particular process, namely, the bonding $\sigma(CN)$ and antibonding $\sigma^*(CN)$ orbitals of the CN bond to be broken. Respectively, the CASSCF wave function is written as a composition with the doubly occupied core orbitals and partially occupied orbitals $\sigma(CN)$ and $\sigma^*(CN)$: [Core]($\sigma$-(CN)$\sigma^*(CN)$)$^2$. As before, the MM subsystem is described by the OPLS-AA parameters. In these calculations, the C–N distance in the quantum fragment served as a reaction coordinate and all other internal coordinates of the QM/MM system were optimized along the reaction path.

The results are shown in Figure 10 by the lower line with squares. It is interesting to follow the changes in conformations of the MM part. Upon separating into two pieces, the helix becomes more and more expanded, as shown in the insets in Figure 10.

To estimate the effect of the MM environment, we computed the dissociation energy curve for the reaction $CH_3$–CO–NH–$CH_3$ → $CH_3$–CO$^\bullet$ + $^\bullet$NH–$CH_3$ completely at the ab initio level by using the same CASSCF methodology. The results are presented by the line with circles in Figure 10. It follows from these simulations that the peptide environment is responsible for about 15% reduction of the dissociation energy of the C–N bond.

**Water Wire in a Polyglycine Analogue of the Gramicidin A.** In the last example, we show that modeling properties of proton wires,[42] namely, the oriented hydrogen-bonded chains of water molecules capable to transform protons inside the so-called ionic channels, can be handled with the present QM/MM method. In recent years, these systems attract considerable attention from the theoretical side.[43] It is believed that hydrogen-bonded interactions between molecular groups of the channel and water molecules may considerably affect reorientation of the chains and as a consequence impact the proton transport. In our simulations, we provide a quantitative estimate of this observation by comparing the potentials of rotation around the hydrogen bond for water molecules inside the channel and in the free state.

From the experimental double-helical structure of the gramicidin A (entry 1C4D of the Protein Data Bank), we derived an initial configuration of its polyglycine analogue by replacing all residues by glycine. The so-obtained polypeptide tube consisted of 30 residues, being about 25 Å in length. In simulations, we considered the channel as a MM subsystem, which, according to our methodology, was partitioned into a
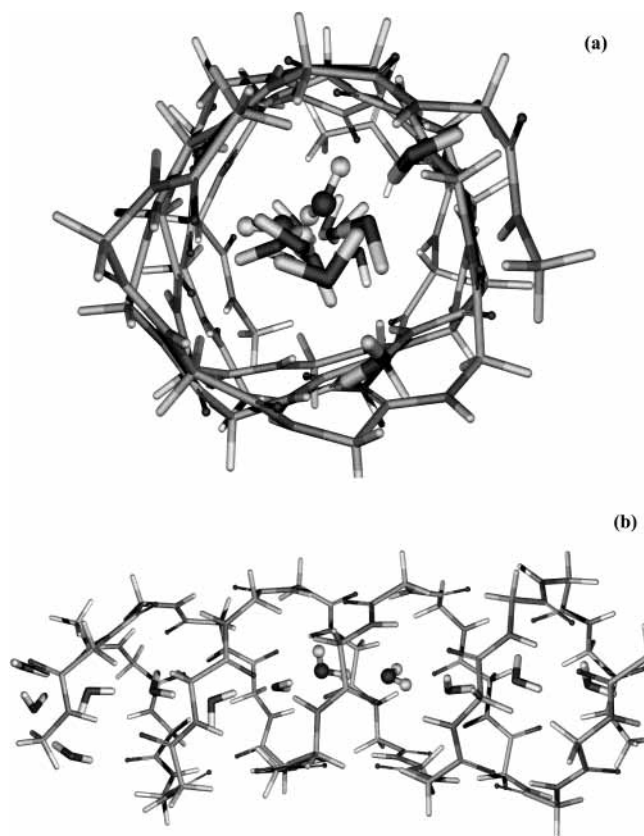


**Figure 11.** Two projections of the equilibrium configuration for the polypeptide channel with the inserted 14 water molecules. In panel b, two water molecules assigned to the QM subsystem are distinguished by balls and sticks and the EFP water molecules are shown in sticks.

flexible chain of 66 effective fragments consisting of 2–4 atoms each. We assumed the partial QM and partial EFP description for the water molecules inserted inside the channel, as explained below. It is worth noting that in this case the QM/MM boundary expands over the hydrogen bonds. We used the Hartree–Fock/6-31G approach for the QM part, the OPLS-AA parameters for the MM part, and the library parameters for the water EFPs included in GAMESS.[13–16]

As a first step in the modeling, we carried out a complete QM/EFP/MM geometry optimization for the peptide tube with 14 water molecules inside the channel. The so-obtained equilibrium configuration of the channel with the water chain is shown in Figure 11.

In this example, we concentrated on such delicate property as the potential of internal rotation of the water dimer around the axis, which almost coincides with the hydrogen bond. More specifically, we varied the dihedral angle $\phi$(H–O–O–H) in the water dimer and for each value of $\phi$ all remaining 11 internal coordinates of $(H_2O)_2$ were optimized. Such a procedure is easy to perform for the water dimer in the absence of any environment. The resulting potential is shown in Figure 12 as a curve with squares. It should be noted that for each curve in the graph the energy zero corresponds to the minimum energy configuration of the particular system. Clearly, relative rotations of water molecules free of surrounding species do not require activation: the rotation barrier is about 0.4 kcal/mol.

To consider rotations in the channel, we selected two water molecules assigned to the QM subsystem (shown in balls and sticks in Figure 11b), while the remaining 12 water molecules on both sides from the central dimer in the chain were treated at the EFP level. Several options were explored in simulations.

Modeling of Biomolecular Systems

*J. Phys. Chem. A, Vol. 106, No. 44, 2002* **10671**
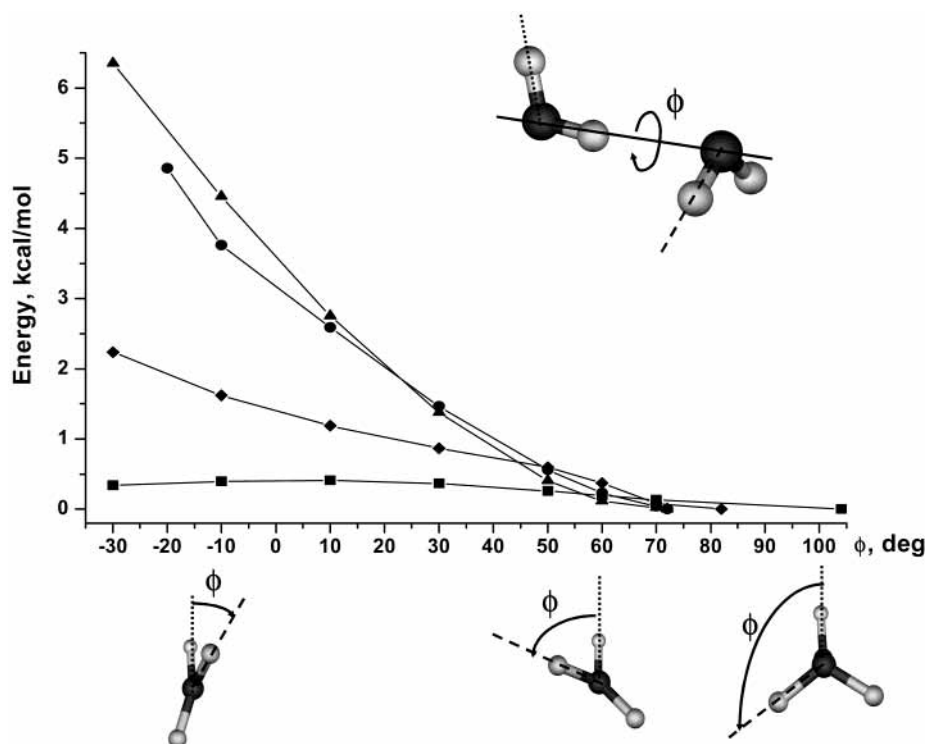


**Figure 12.** The computed section for the potential of internal rotation in the water dimer. The definition of the rotation angle $\phi$ is clarified in the insets. The schemes below the abscissa are the projections of the system shown in the upper inset along the oxygen−oxygen axis (bold line). Then the angle $\phi$ is counted from the dotted line to the dashed line in all insets. In the main graph, the curve with squares refers to the water dimer free from any environment. The curve with diamonds refers to the dimer inside the channel, surrounded by the EFP water molecules, and the positions of all particles in the system are completely optimized at the QM/MM level. The curve with circles corresponds to the water dimer inside the frozen polypeptide tube in the absence of surrounding EFP water molecules. The curve with triangles shows the results for the frozen tube, but the positions of the EFP water molecules are optimized. For each curve in the graph, the energy zero corresponds to the minimum energy configuration of the particular system. In all cases, internal coordinates of the dimer are optimized for every value of $\phi$.

First, we computed the potential at the QM/MM level by optimizing all available coordinates, namely, 11 internal coordinates of the QM water dimer, positions of the 12 EFP water molecules, and positions of all 66 effective fragments constituting the walls of the polypeptide channel. The corresponding potential curve is distinguished by the diamond symbols in Figure 12. An amount of energy required to perform a significant rotation by 120° (see sketches below abscissa in Figure 12) is about 1−2 kcal/mol, which is considerably higher than in the case of free (or gas-phase) water dimer.

This amount increases dramatically, if some of the coordinates of the surrounding particles are frozen at the positions corresponding to the global minimum, as illustrated by the curves with circles and triangles in Figure 12. The curve with triangles shows the results for the frozen polypeptide tube, but the positions of the EFP water molecules are optimized for each value of $\phi$. The curve with circles refers to the simplest simulations, in which 12 EFP water molecules are deleted from the system and positions of effective fragments in the polypeptide channel are fixed. From these simulations, it is clear that a constraint of frozen walls in the channel seriously affects the rotation potential.

The obtained results lead to the important conclusions relevant to modeling properties of water wires. A comparison of the curves with squares and diamonds in Figure 12 shows that the peptide−water environment, even being completely relaxed, seriously restricts the internal rotation in the water dimer. Therefore, a mobility of a water wire inside polypeptide channels should be much less than that in the free state. More detailed discussions on the ab initio and QM/MM potentials for the proton transport along water wires will be presented elsewhere.

## 4. Conclusions

In this work, we demonstrate new perspectives of the EFP-based QM/MM theory for modeling properties and reactivity of large molecular systems of biochemical significance. Namely, it is shown that a restriction of frozen internal coordinates in EFs can be removed by dividing the MM subsystem into a set of small effective fragments and replacing the EFP−EFP interactions by the MM force fields. To solve the QM/MM boundary problem across the covalent bonds, we introduce the buffer fragment, common to both subsystems, and treat it in a specific way when computing energy and energy gradients. The buffer effective fragment, in some sense, keeps the features of both approaches to the QM/MM boundary, link atom, and frozen MOs.[1,7] As a part of quantum subsystem, the buffer fragment is saturated by a link hydrogen atom. On the other hand, the use of localized minimal basis set for the buffer atoms mimics an approximation of frozen MOs. The use of hydrogen as a link atom is not a necessary step in this QM/MM method, and principally, the hydrogen atom can be easily replaced by a pseudoatom. So far, the QM/MM cuts through the $C_\alpha - C_\beta$ covalent bonds have been carefully tested. It is a reasonable approach for a majority of immediate applications for modeling biomolecular systems. Realization of other choices for QM/MM boundaries, for example, including C−N and C−O cuts, is straightforward but will require additional experience.

By applying different quantum chemistry methods (HF, MP2, CASSCF) in conjunction with the MM force fields to the systems described in section 3, we confirm that the effects of protein environment on the processes in the QM active part are more than substantial. The most noticeable is a 2-fold reduction

of the energy difference between ground-state and intermediate-state complexes for the model serine protease system because of the contributions of the MM groups. The surrounding peptide chains seriously modify the sections of potential energy surfaces responsible for dissociation of the C−N bond in a polypeptide and also for rotations about hydrogen bonds of water clusters inside the tube.

## References and Notes

(1) (a) Warshel, A.; Levitt, M. *J. Mol. Biol.* **1976**, *103*, 227. (b) Singh, U. C.; Kollman, P. A. *J. Comput. Chem.* **1986**, *7*, 718. (c) Field, M. J.; Bash, P. A.; Karplus, M. *J. Comput. Chem.* **1990**, *11*, 700. (d) Gao, J. L.; Xia, X. F. *Science* **1992**, *258*, 631. (e) Stanton, R. V.; Hartsough, D. S.; Merz, K. M. *J. Comput. Chem.* **1995**, *16*, 113. (f) Assfeld, X.; Rivail, J.-L. *Chem. Phys. Lett.* **1996**, *263*, 100. (g) Harrison, M. J.; Burton, N. A.; Hillier, I. H. *J. Am. Chem. Soc.* **1997**, *119*, 12285. (h) Woo, T. K.; Margl, P. M.; Blochl, P. E.; Ziegler, T. *J. Phys. Chem. B* **1997**, *101*, 7877. (i) Gao, J.; Amara, P.; Alhambra, C.; Field, M. J. *J. Phys. Chem. A* **1998**, *102*, 4714. (j) Lyne, P. D.; Hodoscek, M.; Karplus, M. *J. Phys. Chem. A* **1999**, *103*, 3462. (k) Shoemaker, J. R.; Burggraf, L. W.; Gordon, M. S. *J. Phys. Chem. A* **1999**, *103*, 3445. (l) Eichinger, M.; Tavan, P.; Hutter, J.; Parrinello, M. *J. Chem. Phys.* **1999**, *110*, 10452. (m) Bryce, R. A.; Vincent, M. A.; Hillier, I. H. *J. Phys. Chem. A* **1999**, *103*, 4094.

(2) (a) Philipp, D. M.; Friesner, R. A. *J. Comput. Chem.* **1999**, *14*, 1468. (b) Murphy, R. B.; Philipp, D. M.; Friesner, R. A. *J. Comput. Chem.* **2000**, *21*, 1442.

(3) (a) Zhang, Y.; Lee, T.-S.; Yang, W. *J. Chem. Phys.* **1999**, *110*, 46. (b) Zhang, Y.; Liu, H.; Yang, W. *J. Chem. Phys.* **2000**, *112*, 3483.

(4) Gogonea, V.; Westerhoff, L. M.; Merz, K. M. *J. Chem. Phys.* **2000**, *113*, 5604.

(5) Hall, R. J.; Hindle, S. A.; Burton, N. A.; Hillier, I. H. *J. Comput. Chem.* **2000**, *21*, 1433.

(6) Sauer, J.; Siekka, M. *J. Comput. Chem.* **2000**, *21*, 1470.

(7) Reuter, N.; Dejaegere, A.; Maigret, B.; Karplus, M. *J. Phys. Chem. A* **2000**, *104*, 1720.

(8) Cui, Q.; Karplus, M. *J. Chem. Phys.* **2000**, *112*, 1133.

(9) Hayashi, S.; Ohmine, I. *J. Phys. Chem. B* **2000**, *104*, 10678.

(10) Houjou, H.; Inoue, Y.; Sakurai, M. *J. Phys. Chem. A* **2001**, *105*, 867.

(11) Cui, Q.; Elstner, M.; Kaxiras, E.; Frauenheim, T.; Karplus, M. *J. Phys. Chem. B* **2001**, *105*, 569.

(12) Laio, A.; Vondele, J. V.; Rothlisberger, U. *J. Chem. Phys.* **2002**, *116*, 6941.

(13) Day, P. N.; Jensen, J. H.; Gordon, M. S.; Webb, S. P.; Stevens, W. J.; Krauss, M.; Garmer, D.; Basch, H.; Cohen, D. *J. Chem. Phys.* **1996**, *105*, 1968.

(14) Gordon, M. S.; Freitag, M. A.; Bandyopadhyay, P.; Jensen, J. H.; Kairys, V.; Stevens, W. J. *J. Phys. Chem. A* **2001**, *105*, 293.

(15) Chen, W.; Gordon, M. S. *J. Chem. Phys.* **1996**, *105*, 11081.

(16) Krauss, M.; Webb, S. P. *J. Chem. Phys.* **1997**, *107*, 5771.

(17) Wadkowski, B. D.; Krauss, M.; Stevens, W. J. *J. Am. Chem. Soc.* **1995**, *117*, 10537.

(18) Krauss, M. *Comput. Chem.* **1995**, *19*, 199.

(19) Krauss, M.; Wadkowski, B. D. *Int. J. Quantum Chem.* **1998**, *69*, 11.

(20) Worthington, S. E.; Krauss, M. *Comput. Chem.* **2000**, *24*, 275.

(21) Roitberg, A. E.; Worthington, S. E.; Holden, M. J.; Mayhew, M. P.; Krauss, M. *J. Am. Chem. Soc.* **2000**, *122*, 7312.

(22) Worthington, S. E.; Roitberg, A. E.; Krauss, M. *J. Phys. Chem. B* **2001**, *105*, 7087.

(23) Worthington, S. E.; Krauss, M. *J. Phys. Chem. B* **2001**, *105*, 7096.

(24) Kairys, V.; Jensen, J. H. *J. Phys. Chem. A* **2000**, *104*, 6656.

(25) Minikis, R. M.; Kairys, V.; Jensen, J. H. *J. Phys. Chem. A* **2001**, *105*, 3829.

(26) Li, H.; Jensen, J. H. *Theor. Chem. Acc.* **2002**, *107*, 211.

(27) Li, H.; Hains, A. V.; Everts, J. E.; Robertson, A. D.; Jensen, J. H. *J. Phys. Chem. B* **2002**, *106*, 3486.

(28) Schmidt, M. W.; Baldridge, K. K.; Boatz, J. A.; Elbert, S. T.; Gordon, M. S.; Jensen, J. H.; Koseki, S.; Matsunaga, N.; Nguyen, K. A.; Su, S. J.; Windus, T. L.; Dupuis, M.; Montgomery, J. A. *J. Comput. Chem.* **1993**, *14*, 1347.

(29) Nemukhin, A. V.; Grigorenko, B. L.; Bochenkova, A. V.; Topol, I. A.; Burt, S. K. *J. Mol. Struct. (THEOCHEM)* **2002**, *581*, 167.

(30) Granovsky, A. A. http://lcc.chem.msu.ru/gran/gamess/index.html.

(31) (a) Ponder, J. W.; Richards, F. M. *J. Comput. Chem.* **1987**, *8*, 1016. (b) Kundrot, C. E.; Ponder, J. W.; Richards, F. M. *J. Comput. Chem.* **1991**, *12*, 402. (c) Dudek, M. J.; Ponder, J. W. *J. Comput. Chem.* **1995**, *16*, 791. (d) Hodsdon, M. E.; Ponder, J. W.; Cistola, D. P. *J. Mol. Biol.* **1996**, *264*, 585. (e) Kong, Y.; Ponder, J. W. *J. Chem. Phys.* **1997**, *107*, 481. (f) Dudek, M. J.; Ramnarayan, K.; Ponder, J. W. *J. Comput. Chem.* **1998**, *19*, 548. (g) Pappu, R. V.; Hart, R. K.; Ponder, J. W. *J. Phys. Chem. B* **1998**, *102*, 9725. (h) http://dasher.wustl.edu/tinker.

(32) Stevens, W. *REPGEN for Optimizing Effective Fragment Repulsive Potentials*; CARB: 1991.

(33) Nemukhin, A. V.; Topol, I. A.; Grigorenko, B. L.; Burt, S. K. *J. Phys. Chem. B* **2002**, *106*, 1734.

(34) Reed, A. E.; Curtiss, L. A.; Weinhold, F. *Chem. Rev.* **1988**, *88*, 899.

(35) Nemukhin, A. V.; Topol, I. A.; Burt, S. K. *Int. J. Quantum Chem.* **2002**, *88*, 34.

(36) Kraut, J. *Annu. Rev. Biochem.* **1977**, *46*, 331.

(37) Warshel, A.; Naray-Szabo, G.; Sussman, F.; Hwang, J.-K. *Biochemistry* **1989**, *28*, 3629.

(38) Daggett, V.; Schröder, S.; Kollman, P. *J. Am. Chem. Soc.* **1991**, *113*, 8926.

(39) Štrajbl, M.; Florian, J.; Warshel, A. *J. Am. Chem. Soc.* **2000**, *122*, 5354.

(40) Betzel, C.; Gourinath, S.; Kumar, P.; Kaur, P.; Perbandt, P.; Eschenburg, S.; Singh, T. P. *Biochemistry* **2001**, *40*, 3080.

(41) Nemukhin, A. V.; Weinhold, F. *J. Chem. Phys.* **1992**, *97*, 1095.

(42) Nagle, J. F.; Morowitz, H. J. *Proc. Natl. Acad. Sci. U.S.A.* **1978**, *75*, 298.

(43) (a) Pomès, R.; Roux B. *Chem. Phys. Lett.* **1995**, *234*, 416. (b) Lobaugh, J.; Voth, G. A. *J. Chem. Phys.* **1995**, *104*, 2056. (c) Pomès, R.; Roux B. *J. Phys. Chem.* **1996**, *100*, 2519. (d) Pomès, R.; Roux B. *Biophys. J.* **1996**, *71*, 19. (e) Sagnella, D. E.; Laasonen, K,; Klein, M. L. *Biophys. J.* **1996**, *71*, 1172. (f) Tuckerman, M. E.; Marx, D.; Klein, M. L.; Parinello, M. *Science* **1997**, *275*, 817. (g) Mei, H. S.; Tuckerman, M. E.; Sagnella, D. E.; Klein, M. L. *J. Phys. Chem. B* **1998**, *102*, 10446. (h) Sagnella, D. E.; Sagnella, D. E. *J. Chem. Phys.* **1998**, *108*, 2073. (i) Pomès, R.; Roux B. *Biophys. J.* **1998**, *75*, 33. (j) Schmitt, U. W.; Voth, G. A. *J. Chem. Phys.* **1999**, *111*, 9361. (k) Sadeghi, R. R.; Cheng, H.-P. *J. Chem. Phys.* **1999**, *111*, 2086. (l) Pomès, R.; Roux B. *Biophys. J.* **2002**, *82*, 2304. (m) Meuwyl, M.; Karplus, M. *J. Chem. Phys.* **2002**, *116*, 2572.